FDTD MODELING OF THE BREAST: A REVIEW

M. O'Halloran, R. Conceição, D. Byrne, M. Glavin and E. Jones

Electronic and Electrical Engineering
National University of Ireland Galway, Ireland

Abstract—Microwave imaging is one of the most promising emerging imaging technologies for breast cancer detection. Microwave imaging exploits the dielectric contrast between normal and malignant breast tissue at microwave frequencies. Many UWB radar imaging techniques require the development of accurate numerical phantoms to model the propagation and scattering of microwave signals within the breast. The Finite Difference Time Domain (FDTD) method is the most commonly used numerical modeling technique used to model the propagation of Electromagnetic (EM) waves in biological tissue. However, it is critical that an FDTD model accurately represents the dielectric properties of the constituent tissues and the highly correlated distribution of these tissues within the breast. This paper presents a comprehensive review of the dielectric properties of normal and cancerous breast tissue, and the heterogeneity of normal breast tissue. Furthermore, existing FDTD models of the breast are examined and compared. This paper provides a basis for the development of more geometrically and dielectrically accurate numerical breast phantoms used in the development of robust microwave imaging algorithms.

1. INTRODUCTION

Breast cancer is one of the most common cancers in women. In the United States alone, it accounts for 26% of new cancer cases, and is second only to lung cancer as the leading cause of deaths among american women [1]. More than 180,000 new cases are diagnosed each year, resulting in more than 40,000 deaths annually [2]. Worldwide, the incidence of breast cancer has increased by 0.5% annually, with 1.35 to 1.45 million new cases projected by 2010 [2]. While comprehensive

---

Corresponding author: M. O'Halloran (martin.ohalloran@gmail.com).

physical examinations, and regular self-examinations contribute to early detection of breast cancer, the current most effective screening method for the detection of breast cancer is X-ray mammography.

However, despite its widespread use as a screening technology, the limitations of X-ray mammography are well known, especially in radiologically dense glandular tissue [2]. X-ray mammography also requires the uncomfortable compression of the breast. Almost 70% of all lesions identified by X-ray mammography are later found to be benign [3]. More worryingly, between 4% and 34% of all breast cancers are missed by traditional X-ray mammography [4]. In younger women in particular, breast tissue typically presents a higher dense-to-fatty tissue ratio and lesions occurring in dense-tissue breasts are statistically more likely to be missed by X-ray mammography [5]. Issues also exist with the alternative imaging technologies to X-ray mammography: MRI and Ultrasound. Despite the fact that recent research has shown that MRI has a negative predictive value of 99% [6], the cost and issues with the sensitivity and specificity of these alternative imaging modalities preclude their widespread use [7, 8].

One of the most promising emerging breast imaging technologies is Microwave imaging, which is non-ionising, does not require breast compression, is less invasive than X-rays and is potentially low cost. The physical basis for microwave imaging is the significant dielectric contrast between normal and malignant breast tissue that exists at microwave frequencies. Three alternative active microwave imaging techniques are under development, Hybrid Microwave-Induced Acoustic imaging, Microwave Tomography and Ultra-Wideband (UWB) Radar imaging. The hybrid imaging method involves heating any tumours present in the breast using microwave signals, and using ultrasound transducers to record the resultant pressure waves due to the heat-induced expansion of the tumour tissue. Based on these recorded waves, the presence and location of the tumours can be identified [9–11]. Microwave Tomography involves reconstructing the complete dielectric profile of the breast using a forward and inverse scattering model [12–17]. Microwave Tomography is limited by resolution, the amount of *a priori* information required, and the significant computational requirement of the imaging technique. Finally, Ultra-Wideband (UWB) Radar imaging, as proposed by Hagness et al. [18], uses reflected UWB signals to determine the location of microwave scatterers within the breast. Rather than using the tomographic approach of reconstructing the entire dielectric profile of the breast, UWB radar imaging, which was originally used in concealed weapon detection systems [19, 20], uses the Confocal Microwave Imaging (CMI) approach [18] to identify and locate regions

of scatterings within the breast [21–29]. Regions of high energy within the resultant images may suggest the presence of cancerous tissue due to the dielectric contrast that exists between normal and cancerous tissue.

All of these imaging approaches require accurate FDTD breast phantoms to model the propagation and scattering of microwave signals within the breast. The FDTD method has become the *de facto* numerical method for modeling the propagation of electromagnetic (EM) signals in biological tissue. FDTD breast models must incorporate the geometrical properties of the breast, the natural heterogeneity of the breast structure and the dispersive properties of breast tissue. The structure of the paper is as follows: Section 2 examines the dielectric properties of the breast (both historical and more recent); Section 3 describes and compares existing FDTD breast models; Section 4 describes the development of accurate tumour models; finally, Section 5 discusses the conclusions and suggestions for future work.

2. DIELECTRIC PROPERTIES OF BREAST TISSUE

An FDTD model of the breast must accurately reflect the dielectric contrast between adipose, fibroglandular and cancerous breast tissue. Several studies of the dielectric properties of breast tissue have been undertaken and a brief overview of the individual findings is presented here: Chaudhary et al. [30] measured the dielectric properties of normal
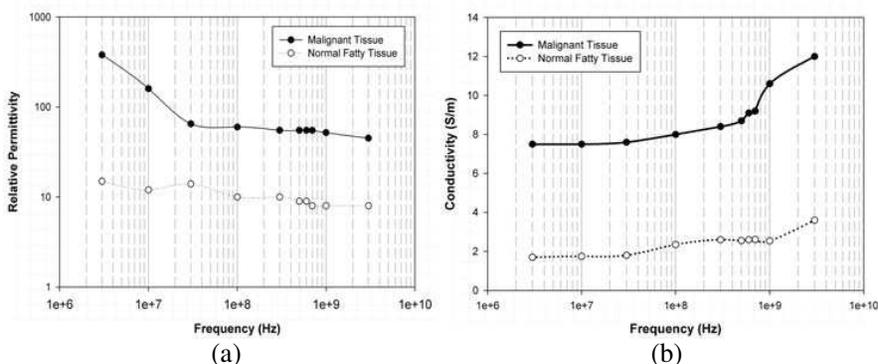

Figure 1. The variation of (a) the relative permittivity, and (b) the conductivity of normal and malignant tissue between 3 MHz and 3 GHz as reported by Chaudhary et al. [30].

and malignant breast tissue between 3 MHz and 3 GHz at 25 °C. The variation of the dielectric properties of normal and malignant tissue with frequency as established by Chaudhary is shown in Figure 1. Chaudhary et al. concluded that significant differences existed in the dielectric properties of normal and malignant tissues of the human breast (4.7 : 1 for conductivity and 5 : 1 for relative permittivity).

Joines et al. [31] measured the dielectric properties of various types of normal and malignant tissue from 50 to 900 MHz. The measured permittivity and conductivity are shown in Figure 2. Across the range of tissues examined, Joines observed the greatest dielectric contrast between normal and malignant tissue for the mammary gland, with an average difference in relative permittivity and conductivity of 6.4 : 1 and 3.8 : 1 respectively, which is in general agreement with the measurements of Chaudhary et al..

Surowiec et al. [32] measured the relative permittivity of infiltrating breast carcinoma and the surrounding tissue at frequencies between 20 kHz and 100 MHz using an automatic network analyser and an end-of-line capacitor sensor. The results were fitted to Cole-Cole dielectric relaxation models [33]. Three categories of tissue were considered by Surowiec:

- The central part of the tumour;
- The tissue immediately surrounding the tumour;
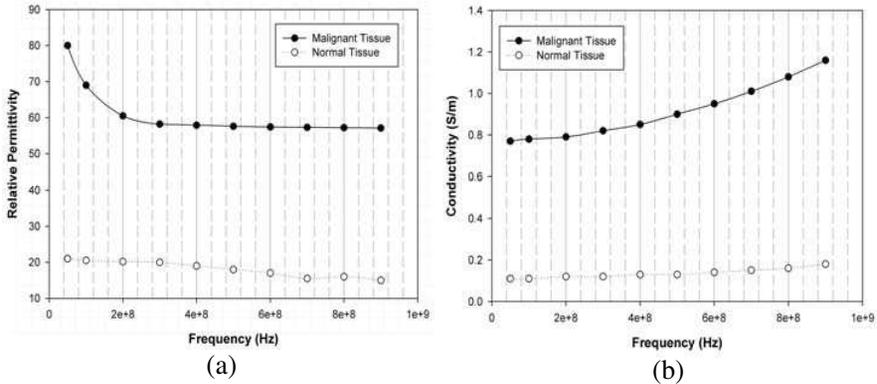- The peripheral tissue at a distance of approximately 2 cm from the centre of the tumour.

(a)   (b)

Figure 2. The variation of (a) the relative permittivity, and (b) the conductivity of normal and malignant tissue between 50 MHz and 900 MHz as reported by Joines et al. [31].
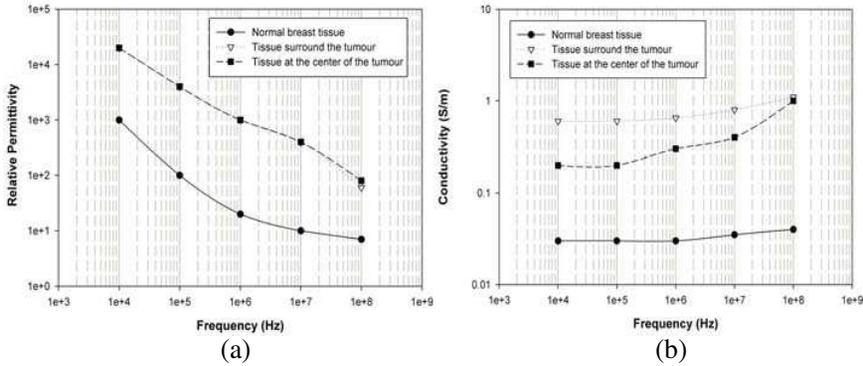
Figure 3. The variation of (a) the relative permittivity, and (b) the conductivity of tumour tissue, the surrounding tissue, and peripheral tissue across the frequency band of 0.02 MHz and 100 MHz as reported by Surowiec et al. [32].

The results of the study are presented in the form of Cole-Cole models. The permittivity and conductivity of the centre of a tumour, the surrounding tissue, and peripheral tissue as reported by Surowiec et al. are shown in Figure 3. Surowiec et al. observed significantly higher permittivity values for the central part of the tumour and the infiltrating margins compared to tissue taken from the periphery of the tumour. Surowiec et al. suggested that the high permittivity associated with the infiltrating margins of the tumour was due to tumour cell proliferation, and could result in a large microwave scattering, allowing for the identification and localisation of small tumours using UWB radar.

Campbell and Land [34] measured the complex permittivity of female breast tissue at 3.2 GHz using the resonant cavity technique. Campbell and Land's specific aim was to provide detailed dielectric properties measurements at 3.2 GHz for microwave thermography applications. Campbell and Land contended that the dielectric measurements made by Surowiec et al. [32] may have been inaccurate at microwave frequencies due to the fact the samples were collected and stored in physiological saline and that the results at microwave frequencies could be more representative of the saline than the breast tissue sample itself. The resonant cavity technique used by Campbell and Land involved observing the change in the resonant frequency and the unloaded quality factor of the cavity when the sample was inserted into one of the apertures. The cavity was designed so that

only small volumes samples were required (approximately $15\,\mathrm{mm}^3$). Four types of tissue were examined: fatty tissue, normal tissue, benign breast tumour tissue and malignant breast tissue. The results are outlined in Table 1. While Campbell and Land noted a significant dielectric contrast between normal (fat tissue and all other breast tissue) and tumourous tissue, they also suggested that due to the similarity in dielectric properties of malignant and benign tumours, it may be impossible to distinguish between the two based on dielectric properties alone. Campbell and Land also noted much greater variance in the dielectric properties of normal tissue than suggested in previous studies. In a more recent study, Choi et al. [35] measured the dielectric properties of breast cancer tissue, along with the properties of metastasised lymph nodes and normal lymph nodes in the frequency band between 0.5 and 30 GHz. The results of the measurements are shown in Figure 4, once again illustrating a dielectric contrast between normal and malignant breast tissue.

Table 1. Dielectric properties of female breast tissue at 3.2 GHz as reported by Campbell and Land [34].

Tissue type	Relative Permittivity	Conductivity (S/m)	Water content (%)
Fatty tissue	2.8–7.6	0.54–2.9	11–31%
Normal tissue	9.8–46	3.7–34	41–76
Benign tissue	15–67	7–49	62–84
Malignant tissue	9–59	2–34	66–79

All of the studies detailed up to this point have been *ex vivo* studies. Next, an *in vivo* method is examined, in which the dielectric properties of normal breast tissue are estimated. Meaney et al. [36] used a clinical prototype of a tomographic microwave imaging system to estimate the dielectric properties of normal breast tissue *in vivo*. Meaney et al. measured the average permittivity and conductivity of cancer-free breast tissue, the results of which are shown in Table 2. Meaney et al. noted that the average permittivity values of normal tissue at 900 MHz are significantly higher than those previously published in the *ex vivo* studies of Joines et al. [31] and Chaudhary et al. [30]. Since Meaney et al. did not examine malignant tissue, a similar comparison of the dielectric properties of *in vivo* and *ex vivo* malignant tissue cannot be made. Meaney et al. also suggested that a correlation existed between the average permittivity values and the radiographic density of the tissue, since patients categorised radiographically as having high fat content tissue had an average permittivity value of 31, while patients categorised as having heterogeneously dense tissue
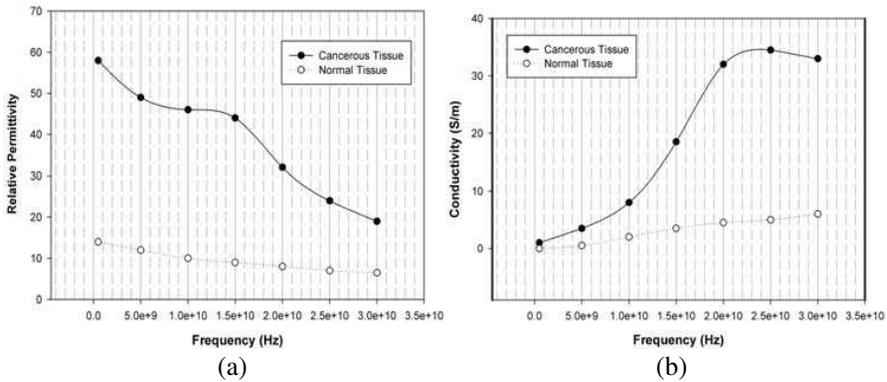
Figure 4. The variation of (a) the relative permittivity, and (b) the conductivity of normal and malignant tissue between 0.5 GHz and 30 GHz as reported by Choi et al. [35].

had average relative permittivities between 35 and 36.

Finally, the most recent, and arguably most comprehensive examination of the dielectric properties of normal and malignant tissue was recently completed by Lazebnik et al. [37, 38]. The aim of Lazebnik's studies was to:

(i) Characterise the dielectric properties of a large number of freshly excised breast reduction, biopsy, lumpectomy and mastectomy tissue across a very wide frequency range from 0.5 to 20 GHz.

(ii) Correlate the measured dielectric properties with histopathological analysis of the tissue samples.

(iii) Perform statistical analysis to ensure the integrity of the data, reduce the data to simple Cole-Cole representations and assist in drawing conclusions.

Table 2. Average dielectric properties of female breast tissue at 900 MHz measured *in vivo* using an active microwave imaging system developed by Meaney et al. [36].

Patient	Age	Average Permittivity	Average Conductivity (S/m)
1	76	17.22 ± 11.21	0.5892 ± 0.3547
2	57	31.14 ± 4.35	0.6902 ± 0.3650
3	52	36.44 ± 6.24	0.6869 ± 0.3156
4	49	35.43 ± 3.93	0.5943 ± 0.3841
5	48	30.85 ± 7.22	0.6350 ± 0.3550

Lazebnik et al. [37, 38] hoped to compensate for some of the apparent weaknesses of previous studies, such as small patient numbers, the fact that many studies did not exceed 3.2 GHz in frequency, and the limited types of tissues examined. One of the most significant differences between Lazebnik et al.'s first study and previous studies was the histological categorisation of the samples. Each sample under consideration was quantified in terms of the percentage of adipose, glandular and fibroglandular tissue present in the sample. In order to effectively summarise the data, Lazebnik et al. formed 3 groups of tissue:

(i) Group 1 contained all samples with 0–30% adipose tissue (99 samples).

(ii) Group 2 contained all samples with 31–84% adipose tissue (84 samples).

(iii) Group 3 contained all samples with 85–100% adipose content (171 samples).

Median permittivity and conductivity curves were created by calculating the fitted values for each sample in the group at 50 equally spaced frequency points. Secondly, the median value at a particular frequency was calculated across all samples within a group. Finally, Cole-Cole equations were used to fit these median values. The Cole-Cole representations for permittivity and conductivity for each tissue group are shown in Figure 5. Lazebnik et al. compared the results of her study with the results of previous studies and her findings were as follows:
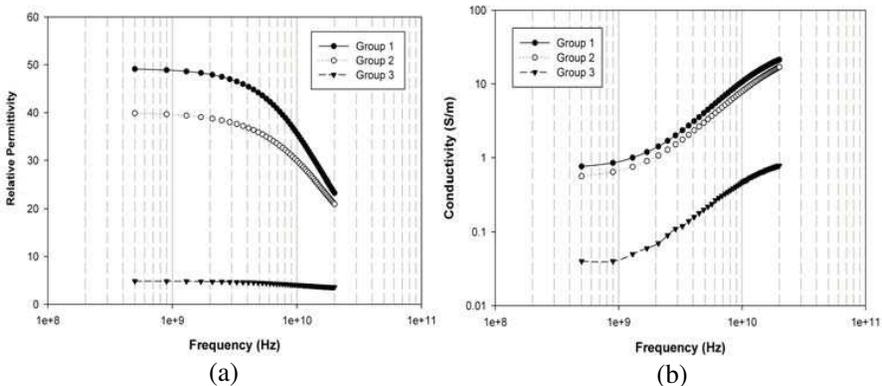

Figure 5. The permittivity (a), and conductivity (b) of normal breast tissue as measured by Lazebnik et al. [37] over the frequency band 0.5 to 20 GHz. Group 1 represents 0–30% adipose tissue, group 2 represents 31–84% adipose and group 3 represents 84–100% adipose tissue.

(i) Lazebnik et al.'s median dielectric curves (permittivity and conductivity) for group 3 tissue was lower than any previously published data for normal tissue, as shown in Figure 6. This tissue consists of between 85 and 100% adipose tissue.

(ii) Lazebnik et al.'s median dielectric curves (permittivity and conductivity) for group 1 tissue was higher than any previously published data for normal tissue. This tissue has a low adipose content between 0 and 30% (due to the high concentration of fibroglandular tissue).

(iii) With the exception of data published by Campbell and Land [34], the dielectric data spanned a much greater range of values than had been reported in smaller scale studies.

Lazebnik et al. attributed these differences to the large heterogeneity in normal breast tissue, as previously noted by Campbell and Land [34]. Lazebnik et al. suggested that the reason this level of heterogeneity was not found in previous studies was the location from which samples of normal tissue had been taken. In previous studies, the samples of normal tissue were taken from regions distinct from the tumour site, and since tumours typically occur in glandular tissue, these normal samples were likely to have a higher adipose content compared to the glandular tissue surrounding the tumour. Therefore, the dielectric heterogeneity of breast tissue was underestimated. Lazebnik et al. also concluded that the dielectric properties of breast tissue were primarily a function of the adipose content of the tissue.

The dielectric properties of normal, benign and malignant breast tissues were further addressed in Lazebnik et al.'s later study [38]. The measured dielectric values for malignant tissue agreed well with previous studies by Chaudhary [30], Surowiec [39] and Joines [31] as shown in Figure 6. Adjusting for adipose content, Lazebnik et al. found only a 10% difference between the conductivity of normal tissue and malignant tissue, and an approximate 8% difference in permittivity at 5 GHz. However, adjusting for adipose and fibroconnective tissue, Lazebnik et al. found no statistical differences between normal glandular and malignant glandular tissues in the breast. This presents a much more difficult imaging scenario than previously assumed.

3. EXISTING FDTD MODELS OF THE BREAST

In this section, existing FDTD breast models are examined. An accurate FDTD model must account for the physical geometry of the breast, the heterogeneity and dispersive nature of normal breast tissue. The design of an FDTD model of the breast depends on the
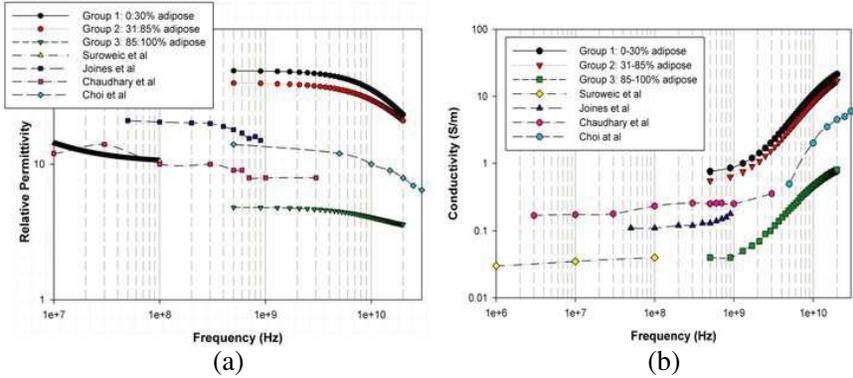
Figure 6. The variation of (a) the permitivity, and (b) the conductivity of malignant breast tissue (solid line) with frequency (reproduced from [37]). Data from previous studies is also shown for comparison.

imaging approach taken. Two different imaging configurations have been considered, the planar configuration used by Hagness et al. [18] and the cylindrical configuration developed by Fear et al. [22].

An imaging configuration is defined by the orientation of the patient and the positions of the antenna array elements. In the planar configuration, the patient is oriented in the supine position with a planar antenna array placed across the naturally flattened breast. Conversely, in the cylindrical configuration, the patient lies in the prone position with the breast naturally extending through an opening in the examination table. A cylindrical array of antennas surrounds the breast. Both the prone and supine positions are shown in Figure 7.

Hagness et al. [18] developed a 2D FDTD model of the breast, based on the planar configuration. Therefore, the model consists of a naturally flattened breast with a tissue depth of 5 cm, which is the typical depth of a normal non-lactating breast. Hagness et al.'s model incorporated normal breast tissue, malignant breast tissue, glandular tissue and veins. The dielectric properties of normal breast used in the FDTD model are based on the dielectric properties as measured by Joines et al. [31] and Chaudhary et al. [30], and extrapolated to higher frequencies by Foster and Schwan [40] using the following Debye Formulation:

$$\varepsilon_r(f) = \varepsilon_\infty + \frac{\varepsilon_s - \varepsilon_\infty}{1 + j(f/f_p)} - \frac{j\sigma}{2\pi f \varepsilon_0} \tag{1}$$
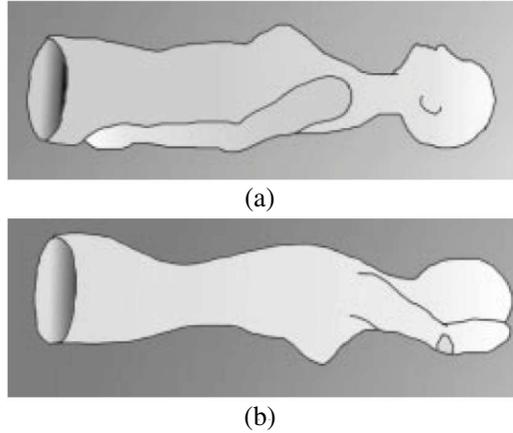
(a)

(b)

Figure 7. The supine patient position is shown in (a), while the prone patient position is shown in (b). This image is reproduced from [22].

Table 3. Permittivity and conductivity variance for normal breast tissue, as established by Joines et al. [31].

Study	Permittivity variance	Conductivity variance
Normal Tissue	$\pm 5\%$	$\pm 7\%$
Malignant Tissue	$\pm 7\%$	$\pm 9\%$

where f is the frequency in Hz, $\varepsilon_s = 10$, $\varepsilon_0 = 8.854 \times 10^{12}$ F/m, $\varepsilon_\infty = 7$, $f_p = 2.5 \times 10^{10}$ Hz and $\sigma = 0.15$ S/m. Malignant tissue is assigned the dielectric properties of $\varepsilon_r = 50$ and $\sigma = 7$ S/m. The heterogeneity of normal breast tissue was incorporated by varying the permittivity and conductivity of normal tissue within the FDTD model, in line with the variance reported from Joines et al. [31] and Chaudhary et al. [30]. The variance of the dielectric properties of normal tissue established by Joines et al. is shown in Table 3. In order to reflect this variance, Hagness et al. randomly assigned a square block of grid cells (spanning 5×5 mm) in the FDTD model with a permittivity value and a conductivity value in a $\pm 10\%$ range centered around the nominal values in a checkerboard pattern, as shown in Figure 8. Hagness et al. also investigated the effect of directly imposed veins and interposed gland clusters. Veins were modeled as having permittivity $\varepsilon_r = 50$, and conductivity $\sigma = 7$ S/m, while glandular tissue was assumed to have dielectric properties 15% higher than those of adipose tissue. 15% was chosen as it is somewhat beyond the upper limit of the measured variability. The boundaries of the FDTD model were terminated by a Perfectly Matched Layer (PML) [41].
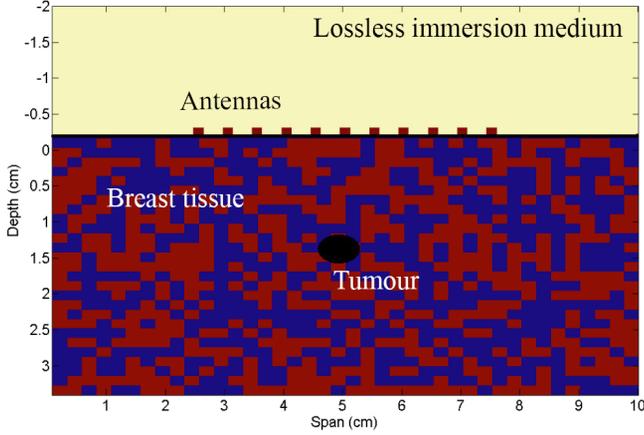
Figure 8. The 2D FDTD model as developed by Hagness et al. [18]. A planar array of antennas is placed across the naturally flattened breast and the dielectric of normal breast tissue are varied by ±10% in a checkerboard pattern.

Fear et al. [42] developed an FDTD model based on the configuration of the patient positioned in the prone position, with the breast extending naturally through a hole in the examination table. The breast is surrounded by a cylindrical array of antennas. The breast itself is modeled as a 6.8 cm diameter cylinder, with a 2 mm layer of skin. The dielectric properties of adipose breast tissue assigned $\varepsilon_r = 9$ and $\sigma = 0.4$ S/m, based on values suggested by Hagness et al. [18]. The dielectric properties of malignant tissues are defined in Fear's model as $\varepsilon_r = 50$ and $\sigma = 4$ S/m. Fear developed a homogeneous and heterogeneous tissue model, as shown in Figure 9. The heterogeneity of breast tissue was incorporated by once again varying the dielectric properties by ±10% around the nominal values, in line with data from Joines et al. [31] and Chaudhary et al. [30]. Fear et al. did not include a Debye formulation, or any other method to model the dispersive nature of breast tissue because she assumed that dispersive or pulse broadening effects of the breast tissue was negligible for the confocal microwave imaging (CMI) approach. It should be noted that in contrast to Hagness's model where the antenna were placed across the surface of the breast, in Fear's model the antennas were placed at a distance of either 1 cm or 2 cm from the surface of the skin.

Li et al. [26] developed an FDTD model of the breast based on actual MRI images of the breast. A high resolution MRI of the breast was taken with the patient in the prone position, and a second low
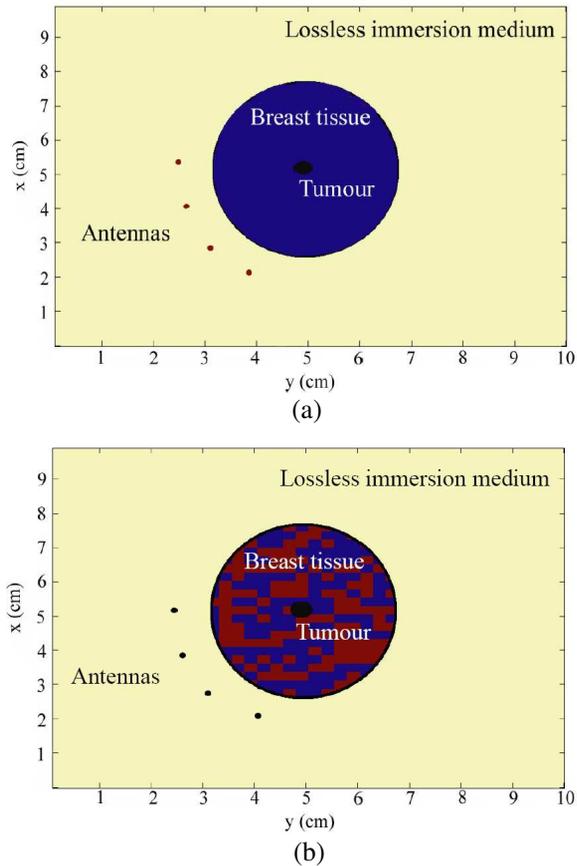
Figure 9. The homogenous cylindrical model (a), and the heterogenous model (b) as developed by Fear et al. [42].

resolution MRI was taken with the patient oriented in the supine position. Li et al. used the low resolution MRI of the patient in the supine position to horizontally expand and vertically compress the high resolution scan, so the overall shape of the high resolution scan matched that of the low-resolution scan. This modified MRI scan clearly shows the distribution of adipose and fibroglandular tissue within the breast, as shown in Figure 10. The dark regions of the MRI represented the adipose tissue, while the lighter regions represented the fibroglandular tissue. The MRI artifacts were removed from the image, and a linear interpolation scheme was used to map the MRI image to the FDTD grid.
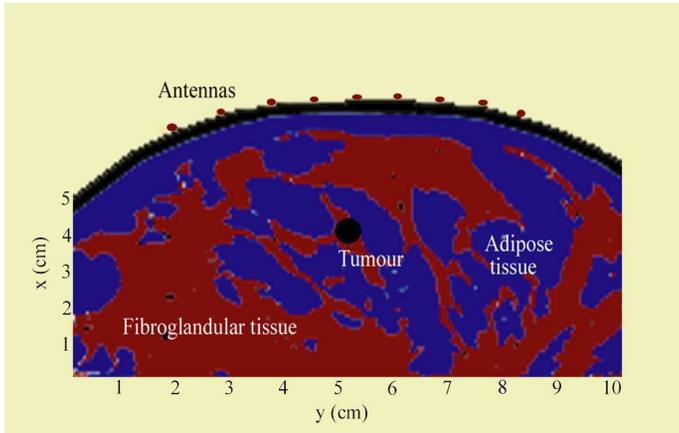
Figure 10. The 2D FDTD model as developed by Li et al. [26]. A planar array of antennas is placed across the naturally flattened breast. The adipose/fibroglandular tissue distribution is clearly visible.

The distribution of adipose and fibroglandular tissue (representing the natural heterogeneity of normal breast tissue) was preserved in the FDTD model by assigning dielectric properties in a $\pm 10\%$ range, based on the intensity values of the corresponding pixels in the MRI. Once again, $\pm 10\%$ around the nominal value was used since it represented the upper bound of breast tissue variability, as reported by Joines et al. [31] and Chaudhary et al. [30]. The dispersive nature of breast tissue was modeled using the Debye formulation (see Equation 1) and incorporated into the FDTD method using an auxiliary differential equation. The Debye parameters for normal tissue were defined as: $\varepsilon_s = 10$, $\varepsilon_\infty = 7$, $\sigma_s = 0.15\,\mathrm{S/m}$ and $\tau = 6.4\,\mathrm{ps}$. The Debye parameters for malignant tissue used by Li et al. [26] are the following: $\varepsilon_s = 50$, $\varepsilon_\infty = 4$, $\sigma_s = 0.7\,\mathrm{S/m}$ and $\tau = 6.4\,\mathrm{ps}$. Skin was assigned the following dielectric values $\varepsilon_r = 36$ and $\sigma = 4\,\mathrm{S/m}$. This modeling procedure developed by Li et al. has since been used by Bond [43], Davis [44], and O'Halloran et al. [45].

Xie et al. [46] developed a 3D hemispherical FDTD model of the breast. The hemisphere was 100 mm in diameter, surrounded by a 2 mm layer of skin. The nipple and the chest wall were also included in the model. To reduce reflections from the skin, the breast model is immersed in a lossless liquid with a permittivity value similar to that of breast tissue. The heterogeneity of breast tissue is modeled by assuming the dielectric properties to be Gaussian random variables with variations of $\pm 10\%$ around the average values, as shown in

Figure 11. The dielectric properties of breast tissue used by Xie et al. are described in Table 4. The dispersive effects of breast tissue is once again incorporated using a Debye formulation, using the parameters established by Li et al. [26]. The grid is terminated by a PML.
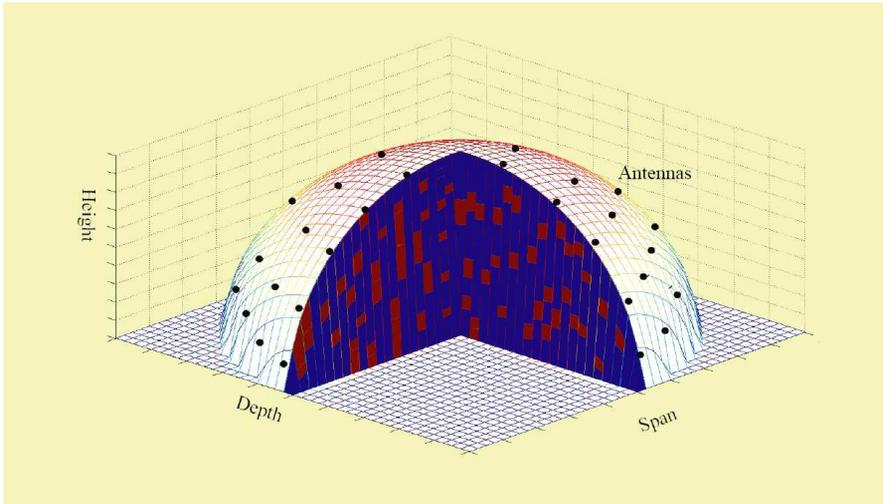

Figure 11. The 3D hemispherical breast model as developed by Xie et al. [46]. The antennas are arranged in P layers with Q antennas per layer surrounding the breast. Once again, the dielectric properties of normal breast tissue are varied by $\pm 10\%$ in a checkerboard pattern.

Table 4. Dielectric properties of breast tissue used in Xie's FDTD model [46].

Tissue	Relative Permittivity	Conductivity (S/m)
Immersion Liquid	9	0
Fatty Breast Tissue	9	0.4
Chest Wall	50	7
Skin	36	4
Nipple	45	5
Glandular Tissue	11–15	0.4–0.5
Tumour	50	4

More recently, a Numerical Breast Phantom Repository has been developed at the University of Wisconsin-Madison, led by Prof. Susan Hagness. The 3D breast phantoms, created from 3D MRIs from patients in the prone position, are composed of a 3D voxel grid where each voxel is defined in terms of its adipose/fibroglandular composition, ranging from $< 25\%$ to $> 75\%$ fibroglandular. In a similar fashion to Li et al.'s 2D FDTD model, the UWCEM Numerical Breast Phantom Repository preserves the highly correlated nature of fibroglandular tissue distribution in the breast, and are much more representative of the structural heterogeneity of normal breast tissue. Moreover, within each breast model, each voxel is defined in terms of tissue type which is mapped to the dielectric properties of normal and malignant breast tissue as established by Lazebnik et al. [37, 38]. An example of the surface of one of the breast models is shown in Figure 12, and a cross section of the model, illustrating the distribution of the various tissues within the breast, is shown in Figure 13.

4. MODELING THE GROWTH PATTERNS AND DIELECTRIC PROPERTIES OF BENIGN AND MALIGNANT BREAST TISSUE

The ability to effectively differentiate between benign and malignant tumours is a key attribute of any successful screening technology, and therefore an accurate numerical model must incorporate these growth patterns and the corresponding dielectric properties. Furthermore, the significant dielectric contrast between adipose and fibroglandular tissue may contribute to non-cancerous high energy regions in UWB radar images, and therefore classification algorithms to further differentiate between normal fibroglandular and malignant tissue need to be developed. With this in mind, methods to incorporate these cancerous growth patterns are examined.

Due to the similarity between the dielectric properties of benign, malignant and glandular breast tissue, as reported by Lazebnik et al. [37, 38], other characteristics inherent to malignant tissue need to be analysed. Across other breast imaging modalities, size, shape, margins, surface texture, depth, localisation and packing density have all been used to identify malignant tissue. However, the most important classification features of a tumour are the shape and texture of the tumour surface. Malignant tumours usually present the following characteristics:

- Irregular, ill-defined and asymmetric shapes;
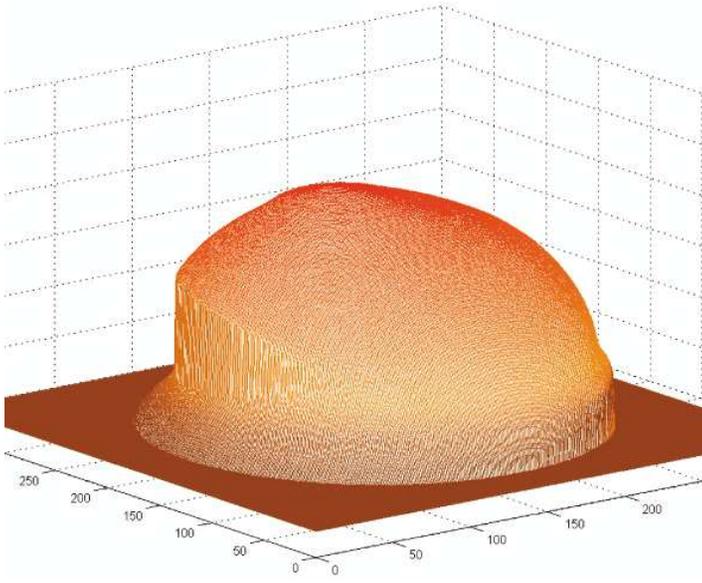- Blurred boundaries (lack of sharpness);

Figure 12. An example of a 3D MRI-derived model of the breast from the UWCEM Numerical Breast Phantom Repository.
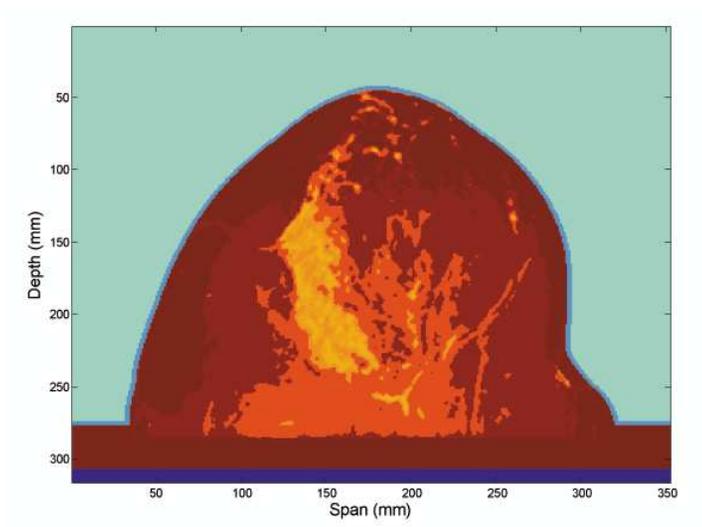

Figure 13. A cross section of an MRI-derived FDTD model highlighting the correlated distribution of tissue within the breast.
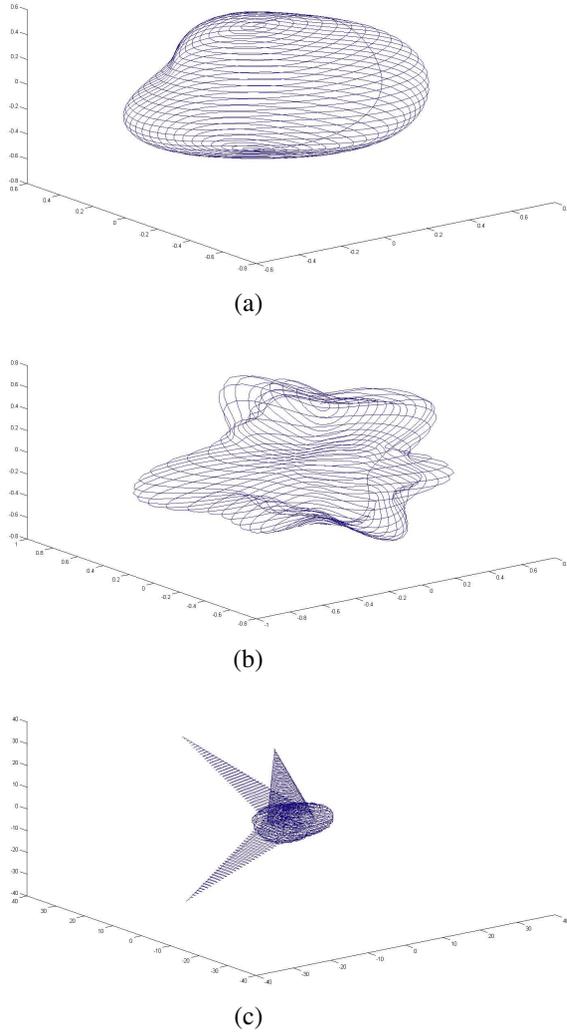
(a)

(b)

(c)

Figure 14. An example of (a) a benign tumour, (b) a lobulated tumour and (c) a spiculated tumour, created using the Gaussian random spheres method.

- Rough and complex surfaces mainly with spicules or microlobules;
- Non-uniform permittivity variations;
- Distortion in the architecture of the breast;

- Irregular increase of tissue density (due to masses and calcifications).

Conversely, benign tumours tend to have the following characteristics:

- Spherical, oval or at least present well-circumscribed contours;
- Compact;
- Smooth surfaces.

In order to develop robust and effective classification algorithms, accurate tumour models need to be developed. The Gaussian random spheres method, as developed by Muinonen et al. [47], and adapted by Davis et al. [48], is used to model the shape and surface texture of both benign and malignant tumours in our 3D breast model. The reason the Gaussian random spheres are used to model tumour growth is that they can be modified mathematically to provide relatively smooth spheres, representative of benign tumours, or alternatively non-regular, ill-defined and asymmetric shapes which are representative of malignant tumour growth patterns.

The Gaussian random spheres are defined by the following equations:

$$r\left(\theta,\psi\right) = ae^{\left[s(\theta,\psi) - \frac{1}{2}\beta^2\right]} \tag{2}$$

where $s\left(\theta,\psi\right)$ is defined as:

$$s\left(\theta,\psi\right) = \sum_{l=0}^{\infty} \sum_{m=-l}^{l} s_{lm} Y_{lm}\left(\theta,\psi\right) \tag{3}$$

where β is the standard deviation of the log-radius, s_{lm} are the spherical harmonics coefficients and Y_{lm} are the orthogonal spherical harmonics.

Examples of smooth, lobulated and spiculated tumour shapes created by the gaussian random spheres method are shown in Figure 14. The origin and growth patterns of these benign and malignant tumours will be established using MRI's of known tumours, guiding the integration of the Gaussian random sphere models into the high fibroglandular content numerical breast phantoms.

5. RESULTS AND CONCLUSIONS

The dielectric properties of the breast, both historical and recent, have been reviewed. Furthermore, existing FDTD breast models, including both 2 dimensional and 3 dimensional phantoms, have been compressively examined and compared.

One of the most significant recent developments is the establishment of the Numerical Breast Phantom Repository at the University of Wisconsin. The phantoms are developed by linearly mapping the various regions of adipose and fibroglandular tissue from high resolution MRIs of the breast to an FDTD grid, and appears one of the most accurate and effective method for modeling the natural heterogeneity of the breast. This method preserves the highly correlated nature of fibroglandular tissue distribution in the breast as described by Kosmas et al. [49], as opposed to the previous methods that model the variance of dielectric properties as being randomly distributed.

Finally, in order to model the shape and growth patterns of tumours within the breast, the Gaussian random spheres method was developed by Davis et al. These models provide representative target backscatter for the development of tumour classification algorithms, such as those developed by Davis et al. [48].

It is hoped that geometrically and dielectrically accurate models, such as the 3D models provided by the UWCEM repository, will become the *defacto* test platform for the development of both UWB imaging algorithms, providing a much more realistic imaging scenario.

ACKNOWLEDGMENT

REFERENCES

1. "Cancer facts and figures 2008," American Cancer Society, 2008.
2. Nass, S. L., I. C. Henderson, and J. C. Lashof, *Mammography and Beyond: Developing Technologies for the Early Detection of Breast Cancer*, National Academy Press, 2001.
3. Elmore, J. G., M. B. Barton, V. M. Moceri, S. Polk, P. J. Arena, and S. W. Fletcher, "Ten-year risk of false positive screening mammograms and clinical breast examinations," *New Eng. J. Med.*, Vol. 338, 1089–1096, 1998.
4. Huynh, P. H., A. M. Jarolimek, and S. Daye, "The false-negative mammogram," *RadioGraphics*, Vol. 18, 1137–1154, 1998.
5. Bird, R. E., T. Wallace, and B. Yankaskas, "Analysis of cancers missed at screening mammograph," *Radiology*, Vol. 184, 613–617, 1992.

6. Lehman, C. D., C. Gatsonis, C. K. Kuhl, and R. E. Hendrick, "MRI evaluation of the contralateral breast in women with recently diagnosed breast cancer," *New Eng. J. Med.*, Vol. 356, No. 13, 1295–1303, Mar. 2007.

7. Viehweg, P., I. Paprosch, M. Strassinopoulou, and S. H. Heywang-Kobrunner, "Contrast-enhanced magnetic resonance imaging of the breast: Interpretation guidelines," *Top. Magn. Reson. Imaging*, Vol. 9, No. 1, 17–43, Feb. 1998.

8. Maestro, C., F. Cazenave, P. Y. Marcy, J. N. Bruneton, and C. Chauvel, "Systematic ultrasonography in asymptomatic dense breasts," *Eur. J. Radiol.*, Vol. 26, No. 3, 254–256, Feb. 1998.

9. Wang, L., X. Zhao, H. Sun, and G. Ku, "Microwave-induced acoustic imaging of biological tissues," *Rev. Sci. Instrum.*, Vol. 70, No. 9, 3744–3748, 1991.

10. Li, D., P. M. Meaney, T. Raynolds, S. A. Pendergrass, M. W. Fanning, and K. D. Paulsen, "Parallel-detection microwave spectroscopy system for breast cancer imaging," *Rev. Sci. Instrum.*, Vol. 75, No. 7, 2305–2313, 2004.

11. Kruger, R. A., K. D. Miller, H. E. Reynolds, W. L. Kiser, D. R. Reinecke, and G. A. Kruger, "Breast cancer in vivo: Contrast enhancement with thermoacoustic CT at 434 MHz — feasibility study," *Radiology*, Vol. 216, No. 1, 279–283, 2000.

12. Bulyshev, A., S. Y. Semenov, A. E. Souvorov, R. H. Svenson, A. G. Nazorov, Y. E. Sizov, and G. P. Tatsis, "Computational modeling of three-dimensional microwave tomography of breast cancer," *IEEE Trans. Biomed. Eng.*, Vol. 48, No. 9, 1053–1056, Sept. 2001.

13. Meaney, P. M., M. W. Fanning, D. Li, S. P. Poplack, and K. D. Paulsen, "A clinical prototype for active microwave imaging of the breast," *IEEE Trans. Microwave Theory Tech.*, Vol. 48, No. 11, 1841–1853, Nov. 2000.

14. Meaney, P. M. and K. D. Paulsen, "Nonactive antenna compensation for fixed array microwave imaging — Part II: imaging results," *IEEE Trans. Med. Imag.*, Vol. 18, No. 6, 508–518, Jun. 1999.

15. Souvorov, A., A. E. Bulyshev, S. Y. Semenov, R. H. Svenson, and G. P. Tatis, "Two dimensional analysis of a microwave flat antenna array for breast cancer tomography," *IEEE Trans. Microwave Theory Tech.*, Vol. 48, No. 8, 1413–1415, Aug. 2000.

16. Bulyshev, A. E., S. Y. Semenov, A. E. Souvorov, R. H. Svenson, A. G. Nazarov, Y. E. Sizov, and G. P. Tatis, "Computational modeling of three-dimensional microwave tomography of breast

cancer," *IEEE Trans. Microwave Theory Tech.*, Vol. 48, No. 9, 1053–1056, Sept. 2001.

17. Liu, Q. H., Z. Q. Zhang, T. Wang, J. A. Byran, G. A. Ybarra, L. W. Nolte, and W. T. Joines, "Active microwave imaging 1-2d forward and inverse scattering methods," *IEEE Trans. Microwave Theory Tech.*, Vol. 50, 123–133, Jan. 2002.

18. Hagness, S. C., A. Taflove, and J. E. Bridges, "Two-dimensional FDTD analysis of a pulsed microwave confocal system for breast cancer detection: Fixed focus and antenna array sensors," *IEEE Trans. Biomed. Eng.*, Vol. 45, 1470–1479, 1998.

19. Sha, L., E. R. Ward, and B. Stroy, "Confocal, synthetic-impulse, millimeter wave system for imaging concealed dielectric and metallic objects," *Proc. North American Radio Science Meeting*, Montreal, Canada, Jul. 1997.

20. Enk, J. O., G. T. Dubiel, and J. E. Bridges, "Millimeter-wave FM radar weapons detection system," *Final Report*, FAA Contract DTFA03-87-C00056, Jul. 1992.

21. Hagness, S. C., A. Taflove, and J. E. Bridges, "Three-dimensional FDTD analysis of a pulsed microwave confocal system for breast cancer detection: Design of an antenna array element," *IEEE Trans. Antennas and Propagat.*, Vol. 47, 783–791, May 1999.

22. Fear, E. C., X. Li, S. C. Hagness, and M. A. Stuchly, "Confocal microwave imaging for breast cancer detection: Localization of tumors in three dimensions," *IEEE Trans. Biomed. Eng.*, Vol. 47, 812–812, 2002.

23. Fear, E. C. and M. A. Stuchly, "Microwave system for breast cancer detection," *New Eng. J. Med.*, Vol. 9, 470–472, Nov. 1999.

24. Fear, E. C., J. Sill, and M. A. Stuchly, "Experimental feasibility study of confocal microwave imaging for breast cancer detection," *IEEE Trans. Microwave Theory Tech.*, Vol. 51, 887–892, Mar. 2003.

25. Fear, E., J. Sill, and M. Stuchly, "Microwave system for breast tumor detection: Experimental concept evaluation," *IEEE AP-S International Symposium and USNC/URSI Radio Science Meeting*, San Antonio, Texas, Jun. 2002.

26. Li, X. and S. C. Hagness, "A confocal microwave imaging algorithm for breast cancer detection," *IEEE Microwave and Wireless Components Letters*, Vol. 11, 130–132, 2001.

27. Li, X., E. J. Bond, and S. H. B. Veen, "An overview of ultra-wideband microwave imaging via space-time beamforming for early-stage breast-cancer detection," *IEEE Antennas and*

Propagation Magazine, Vol. 47, No. 1, 19–34, Feb. 2005.

28. Craddock, I. J., R. Nilavalan, J. Leendertz, A. Preece, and R. Benjamin, "Experimental investigation of real aperture synthetically organised radar for breast cancer detection," *IEEE AP-S International Symposium*, Washington, DC, 2005.

29. Hernandez-Lopez, M., M. Quintillan-Gonzalez, S. Garcia, A. Bretones, and R. Martin, "A rotating array of antennas for confocal microwave breast imaging," *Microw. Opt. Technol. Lett.*, Vol. 39, 307–311, 2003.

30. Chaudhary, S. S., R. K. Mishra, A. Swarup, and J. M. Thomas, "Dielectric properties of normal and malignant human breast tissue at radiowave and microwave frequencies," *Indian J. Biochem. Biophys.*, Vol. 21, 76–79, 1994.

31. Joines, W., Y. Zhang, C. Li, and R. L. Jirtle, "The measured electrical properties of normal and malignant human tissues from 50 to 900 MHz," *Med. Phys.*, Vol. 21, 547–550, 1993.

32. Surowiec, A. J., S. S. Stuchly, J. R. Barr, and A. Swarup, "Dielectric properties of breast carcinoma and the surrounding tissues," *IEEE Trans. Biomed. Eng.*, Vol. 35, No. 4, 257–263, 1988.

33. Taflove, A. and S. C. Hagness, *Computational Electrodynamics: The Finite-difference Time-domain Method*, Artech House Publishers, Jun. 30, 2005.

34. Campbell, A. M. and D. V. Land, "Dielectric properties of female human breast tissue measured in vitro at 3.2 GHz," *Phys. Med. Biol.*, Vol. 37, 193–210, 1992.

35. Choi, J. W., J. Cho, Y. Lee, J. Yim, B. Kang, K. K. Oh, W. H. Jung, H. J. Kim, C. Cheon, H. Lee, and Y. Kwon, "Microwave detection of metastatasized breast cancer cells in the lymph node; potential application for sentinel lymphadenectomy," *Breast Cancer Research and Treatment*, Vol. 86, 107–115, 2004.

36. Meaney, P. M., M. W. Fanning, D. Li, S. P. Poplack, and K. D. Paulsen, "A clinical prototype for active microwave imaging of the breast," *IEEE Trans. Microwave Theory Tech.*, Vol. 48, 1841–1853, 2000.

37. Lazebnik, M., L. McCartney, D. Popovic, C. B. Watkins, M. J. Lindstrom, J. Harter, S. Sewall, A. Magliocco, J. H. Booske, M. Okoniewski, and S. C. Hagness, "A large-scale study of the ultrawideband microwave dielectric properties of normal breast tissue obtained from reduction surgeries," *Phys. Med. Biol.*, Vol. 52, 2637–2656, 2007.

38. Lazebnik, M., D. Popovic, L. McCartney, C. B. Watkins,

M. J. Lindstrom, J. Harter, S. Sewall, T. Ogilvie, A. Magliocco, T. M. Breslin, W. Temple, D. Mew, J. H. Booske, M. Okoniewski, and S. C. Hagness, "A large-scale study of the ultrawideband microwave dielectric properties of normal, benign and malignant breast tissues obtained from cancer surgeries," *Phys. Med. Biol.*, Vol. 52, 6093–6115, 2007.

39. Stuchly, M. A. and S. S. Stuchly, "Dielectric properties of biological substances-tabulated," *J. Microwave Power*, Vol. 14, No. 1, Sept. 1980.

40. Foster, K. R. and H. P. Schwan, "Dielectric properties of tissues and biological materials: A critial review," *Crit. Rev. Biomed. Eng.*, Vol. 17, 25–104, 1989.

41. Berenger, J. P., "A perfectly matched layer for the absorption of electromagnetic waves," *Journal of Computational Physics*, Vol. 114, 185–200, 1994.

42. Fear, E. C. and M. A. Stuchly, "Microwave detection of breast cancer," *IEEE Trans. Microwave Theory Tech.*, Vol. 48, No. 3, 1984–1863, 2000.

43. Bond, E. J., X. Li, S. C. Hagness, and B. D. Van Veen, "Microwave imaging via space-time beamforming for early detection of breast cancer," *IEEE Trans. Antennas and Propagat.*, 1690–1705, 2003.

44. Davis, S. K., E. J. Bond, X. Li, S. C. Hagness, and B. D. Van Veen, "Microwave imaging via space-time beamforming for early detection of breast cancer: Beamformer design in the frequency domain," *Journal of Electromagnetic Waves and Applications*, Vol. 17, 357–381, 2003.

45. O'Halloran, M., M. Glavin, and E. Jones, "Quasi-multistatic MIST beamforming for the early detection of breast cancer," *IEEE Trans. Biomed. Eng.*, in press.

46. Xie, Y., B. Guo, L. Xu, J. Li, and P. Stoica, "Multi-static adaptive microwave imaging for early breast cancer detection," *IEEE Trans. Biomed. Eng.*, Vol. 53, 1647–1657, 2006.

47. Mishchenko, M. I., J. W. Hovenier, and L. D. Travis, *Scattering by Nonspherical Particles: Theory, Measurements and Applications*, Academy Press, 2000.

48. Davis, S. K., B. D. Van Veen, S. C. Hagness, and F. Kelcz, "Breast tumor characterization based on ultrawideband backscatter," *IEEE Trans. Biomed. Eng.*, in press.

49. Kosmas, P., C. M. Rappaport, and E. Bishop, "Modeling with the fdtd method for microwave breast cancer detection," *IEEE Trans. Microwave Theory Tech.*, Vol. 52, 1890–1897, Aug. 2004.